Multi-scale simulations with complex automata: in-stent restenosis and suspension flow

Lorenz, E.

Publication date
2010

Chapter 5

Particle Clustering in Shear-Thickening Hard-Sphere Suspensions

In this chapter a more detailed look at the microstructure and its dynamics of non-Brownian suspensions of monodisperse neutrally buoyant hard-spheres is taken.

5.1 Microstructure of Sheared Suspensions

At low particle Reynolds numbers $Re = 4\dot{\gamma}R_p/\nu_\mathrm{f}$ the behavior of viscous suspensions is relatively well understood. In the dilute limit, hydrodynamic interactions between the particles can be neglected and the suspension exhibits Newtonian rheology with a relative viscosity $\nu_\mathrm{app}/\nu_\mathrm{f} = 1 + 2.5\phi$, where ν_app is the apparent viscosity of the suspension and ν_f the constant viscosity of the suspending fluid. For larger volume fractions ϕ the relative viscosity is well characterized by the Krieger-Dougherty relation (4.1) describing the non-linear increase of the apparent viscosity with the increase of solid volumes in the system. The relation (4.1) is semi-empirical. When leaving the Stokes limit the understanding of the suspension's behavior can be even less supported by analytical derivations. Simulations offer to study the dynamics of the mesoscopic particles and the suspending fluid and serve as an important tool to probe particle microstructure in flow. Parallel to experimental works [199] simulation studies have explored the structural asymmetry [119] and related this to shear-induced normal stresses [117, 200, 201].

In the dilute limit, simple-shear flow with finite shear rates over a sphere was considered using matched asymptotic expansions in the Stokes limit [202]. In this work it was found that weak inertia causes an increase in the particle contribution to the viscosity scaling as $Re^{3/2}$ and the breaking of the symmetry of the Stokes flow particle trajectories which was related to the increase of normal stresses scaling with Re. In addition it is found that inertial effects give rise to a non-isotropic normal stress. Single particles and their positive effect on the apparent viscosity have also been studied in [203]. In the same work it was also observed that for $Re > 1$ the angular velocity of single particles as well as that of clusters of particles decreases

which is then shown to be correlated with the increase of the viscosity.

Expressing the suspension microstructure through the pair-distribution function with the help of accelerated Stokesian dynamics in [201] it is demonstrated how the resulting anisotropy in the pair-distribution function is correlated with the non-Newtonian behavior of the suspension. Allowing for fully resolved flow fields, and therefore for a maximum of realism describing hydrodynamical interactions between particles, the Lattice-Boltzmann method (LBM) has been used to study several aspects of sheared suspensions. In two-dimensional systems the hydrodynamical interaction of pairs of particles and the consequences on their trajectory have been examined [149, 204]. Detailed motion of of isolated particles was studies in [205] and the authors could show how fluid inertia changes the trajectories of particle pairs in simple shear flow. In this work closed trajectories [206] of particles approaching in Stokes flow have been found to be replaced by spiraling and reversing trajectories for $Re > 1$. The authors also discuss how Reynolds stress due to fluctuational motion and stress due to particle acceleration are caused by inertia as an additional mechanism for momentum transport. In [207, 208] distributions of gap widths between particles was studied and found that particle-particle distances become ever smaller with higher shear rates leading to a divergence of inter-particle forces. The resulting shear-thickening behavior was also investigated by means of LBM [115, 103]. In [115] it was found that shear thickening is related to the enhanced contribution from the solid phase to the total shear stress as Re increases. In [209] the clustering of particles in a sheared suspension at Reynolds numbers up to 10 was studied and the increased particle clustering was argued to lead to the increase in viscosity of the suspension. The clustering of suspended particles as the main mechanism leading to shear-thickening was also identified in [102, 103, 208].

In studies of suspension rheology so far attention was mostly paid to the suspensions response to variations of the volume fraction ϕ in the Stokes limit and/or the particle Reynolds number $Re \sim \dot{\gamma}$. In this work we will concentrate on the effect of particle inertia on microstructure and shear-thickening of the suspension by varying the ratio $M = \rho_s/\rho_f$ between the mass density of the solid phase ρ_s and that of the fluid ρ_f of a dense suspension system of which particles occupy a volume fraction $\phi = 0.4$. The mass densities ρ_s and ρ_f apply only to the inertia of the corresponding phase. Gravitational effects were not implemented resulting in a neutrally-buoyant system. The volume fraction was chosen such that it is high enough to undergo clearly visible continuous shear-thickening (disorder→order transition) but low enough not to show ordering effects and discontinuous shear-thickening (order→disorder transition) present for $\phi > \phi_c \gtrapprox 0.6$[1].

5.1.1 Simulations

Using the LB methods described in Sec. 4.4.1 we carried out shear-flow simulations of 2-dimensional neutrally-buoyant monodisperse hard-sphere suspensions with a Newtonian suspending fluid. Within this framework the improved momentum exchange algorithm [210] (or see Sec. 4.4.3) was used to restore Galileian invariance of the LBM particles. To shear the suspension we applied Lees-Edwards boundary conditions [113] as described in Sec. 4.4.2. Lees-Edwards boundary conditions

[1] An exact value for the critical volume fraction marking the crossover between continuous and discontinuous shear-thickening is not known to us for 2D but should be higher than that for 3D, $\phi_c^{3D} \approx 0.55$. See also Sec. 4.1

(LEbc) are particularly useful in studies of a suspensions microstructure since it is not necessary to introduce impenetrable moving walls to drive the shear flow. Thus the particles can freely move in a homogeneous quasi-infinite system. Of course, finite-size effects will set in when the correlation length (e.g. the typical size of particle clusters) in the system reaches the dimensions of the simulation box. We set the system size to $L_x \times L_x = 259 \times 259$ and the particle radius to $R_p = 8.044$ to maximize the reachable Reynolds number which is limited by the typical cluster size to expect[2] and on the Mach number constraint while keeping the accuracy of the spatial resolution at a rather high level. Lubrication corrections were applied to the force and torque of the particles whenever particles come so close that the fluid between them can not be resolved by LBM (see Sec. 4.4.1). However, the dynamics of pressure, velocity and stress field of the fluid between particles might deviate considerably from the pure two-particle assumption in dense suspensions (see also Sec. 4.4.3). Aiming at investigations of the microstructure we chose for the higher resolution over reduction of computational costs. In all simulations of suspensions reported here a number of 132 particles was suspended in the fluid resulting in a volume fraction $\phi = 0.4$. The statistics presented in this chapter were obtained over a total strain of $\dot{\gamma}t = 100$ for all combinations of M and $\dot{\gamma}$. For the lowest shear rates considered, $\dot{\gamma} = 1 \cdot 10^{-5}$, a CPU time of approximately 72 hours were necessary. Measurements were carried after strains of 0.5.

5.1.2 Geometrical properties of Particle Clusters

In Fig. 5.1 snapshots from the evolution of sheared suspensions with solid-fluid mass density ratios $M = \rho_s/\rho_f = 1, 10, 100$ are shown for low ($Re = 0.0155$) and high ($Re = 1.5529$) shear particle Reynolds numbers. At low Reynolds numbers particles hydrodynamically interact at comparatively larger distances. As for the Stokes flow limit, the small pressure increase between two slowly approaching particles is sufficient to maintain distances seldom less than $\approx R_p/5$. At medium Stokes numbers $St \sim MRe$ particle inertia leads to closer particle approaches and particles begin to cluster in small chains connected by regions of short-range deviations from the average fluid pressure. At higher St particle clusters grow longer and wider, and also the correlation length of fluid pressure increases.

In the simulations we recorded the statistics of particle-particle separation vectors. From the magnitude of such vectors it was determined if particle pairs fulfill the cluster condition, i.e. $r_{12} < 2.2 \cdot R_p$ where $r_{12} = |\mathbf{r}_2 - \mathbf{r}_1|$ is the distance between the centers of the particles. This criterion is derived from the observation that the pair-distribution function $g(\mathbf{r}_{12})$ has a maximum at this distance. Applying this cluster condition we aim to identify those particles that have a strong hydrodynamical bond with each other. The strength of hydrodynamical inter-particle friction[3] diverges as $\sim (r_{12} - 2R_p)^{-1}$ the closer the gap between the particles.

[2] which should not be larger than half the system size to minimize the possibility of percolating clusters which would lead to diverging stresses in shear flow

[3] It is possible to term this interaction 'friction' because for small $\mathbf{r}_{12}$ it scales linearly with the relative velocity $\mathbf{F} \sim -\dot{\mathbf{r}}_{12}$.

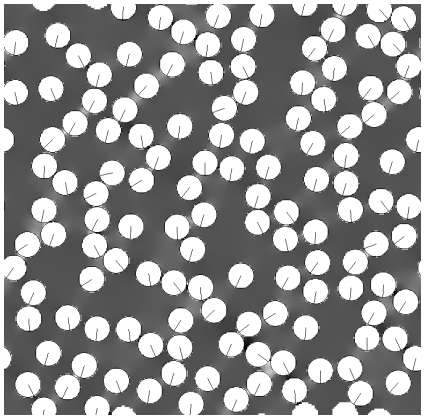

(a) $M = 1$, $Re = 0.0155$

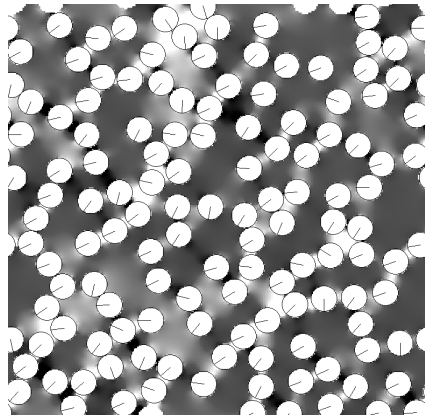

(d) $M = 1$, $Re = 1.5529$

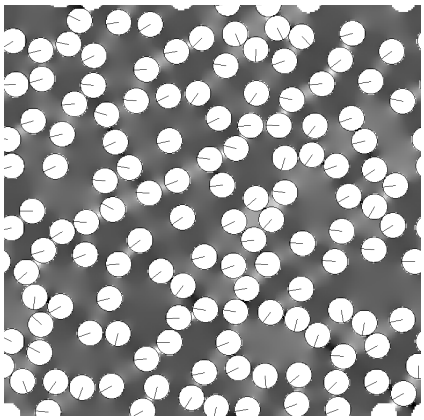

(b) $M = 10$, $Re = 0.0155$

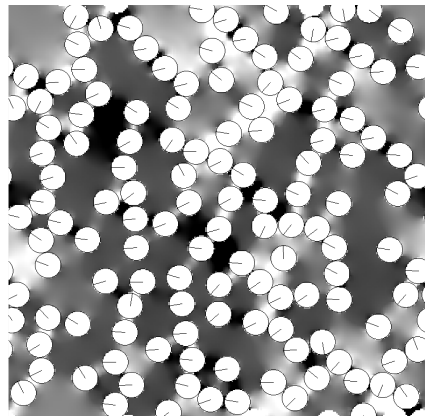

(e) $M = 10$, $Re = 1.5529$

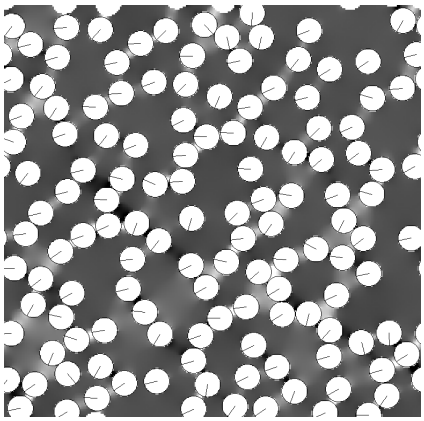

(c) $M = 100$, $Re = 0.0155$

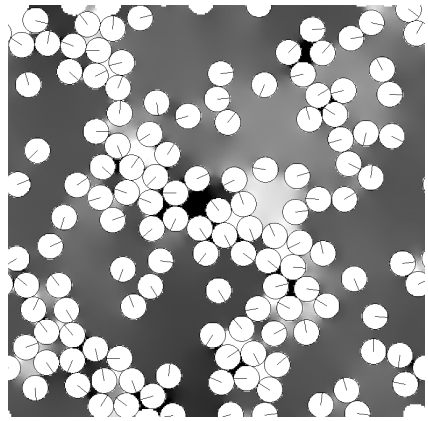

(f) $M = 100$, $Re = 1.5529$

Figure 5.1: Snapshots of sheared suspensions with a volume fraction $\phi = 0.40$ for different values of mass density ratio M and Reynolds numbers. Darker areas of the fluid correspond to higher pressure. The shear is that way that fluid and particles at the top border move to the right and those at the lower border in approximately the same speed to the left.

Cluster Pair Distribution Function

In contrast to the classical pair distribution function $g(\mathbf{r}_{12})$ which takes every possible pair of particles into account, we measured a cluster pair distribution function defined as the probability to find another particle inside the same cluster at a separation $\mathbf{r}_{12}$. In Fig. 5.2 such cluster pair distributions are shown for small and large Reynolds numbers and mass density ratios $M = 1, 10, 100$. In contrast to the classical pair distribution secondary rings of high probability can be clearly found for distances a multiple of $2R_p$ which makes it possible to investigate strength and orientational tendencies of particle clustering. For $M = 1$ we find hardly any change with the Reynolds number. The still relatively low Reynolds number does not lead to a clearly visible asymmetry in the pair distribution which can be found for larger Re (see for example [205, 201, 200, 211]). This corresponds to the still rather uncorrelated distribution of particles in Fig. 5.1(d). When the mass density ratio is increased to $M = 10$ an asymmetry can be clearly found for $Re = 1.5229$. Also, for these parameters an overall increase of the probability can be observed. Corresponding to that, in [200] it was found that $g(\mathbf{r}_{12}) \sim Pe^{0.7} \sim Re^{0.7}$ in direction of compression. Both facts are related to the onset of formation of chain-like particle clusters that are mostly aligned in the compression direction of the shear flow. For $M = 100$, while at $Re = 0.0155$ no changes can be found to the measurements for the smaller M, at the high Reynolds number the asymmetry effect is clearly present as well as an increased probability to find cluster pairs also at larger distances. The asymmetry in Fig. 5.2(f) is comparable to that in Fig. 5.2(e) but a fuzzy fifth ring becomes visible. This suggests that principle geometrical characteristics of particle cluster do not change with increasing typical size.

Fractal Dimension of Particle Clusters

From the statistics we obtained on the particle clusters the probability to find clusters of a certain mass N, i.e. the number of particles in the cluster, and of a radius of gyration R is shown in Fig. 5.3 for the same subset of M and Re. Together with it the two extreme cases of cluster forms are plotted in dashed lines. The line corresponds to the increase of R with N for a perfect chain of particles whereas the lowest curve shows the behavior of R with N for the most compact disk-shaped agglomeration of particles in a perfect hexagonal packing. Regardless the parameters M and Re, the cloud of higher probability to find a cluster of mass N and dimension R can be found closer to the case of chain-like than that of compact cluster shape. Hardly any cluster can be found that could be characterized as compact. The probability distribution has a maximum for $N = 1$ and $R = 2R_p$ which means that still most of the particles are well separated from all other particles. However, for larger M and Re the probability increases to find larger clusters as well while the mean of the distribution follows a power law $R \sim N^{1/D}$. The fractal dimension D could be found to agree for all combinations of M and Re within statistical errors. Its mean could be determined to $D = 1.15$ illustrating the sparse volume occupation of particle clusters. This together with the condition that particles have to be 'connected' implies that clusters tend to be more of chain-like shape.

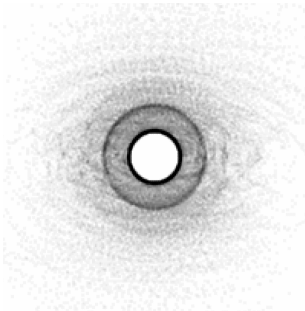

(a) $M = 1$, $Re = 0.0155$

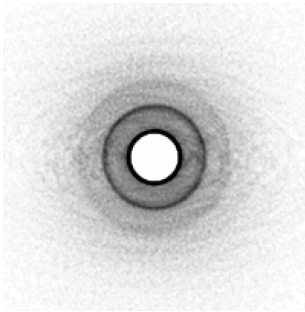

(b) $M = 10$, $Re = 0.0155$

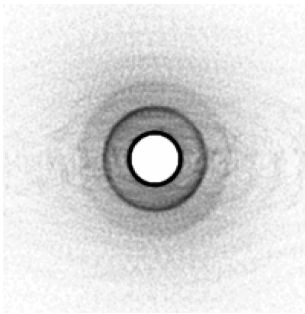

(c) $M = 100$, $Re = 0.0155$

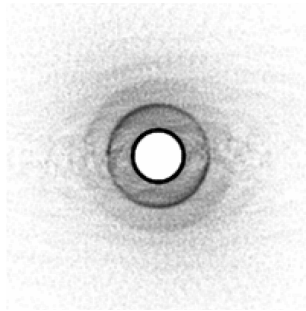

(d) $M = 1$, $Re = 1.5529$

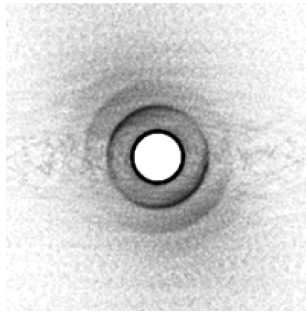

(e) $M = 10$, $Re = 1.5529$

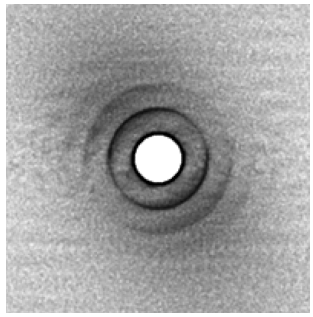

(f) $M = 100$, $Re = 1.5529$

Figure 5.2: Cluster pair distribution function for a subset of considered parameters M and Re taking into account all particles in the same cluster as the reference particle. At low St the distribution of cluster pairs is almost isotropic while for larger St the strength of anisotropy increases. The probability to find another particle in the compression direction increases with higher momentum faster than the probability to find particles of the same cluster in direction of extension.

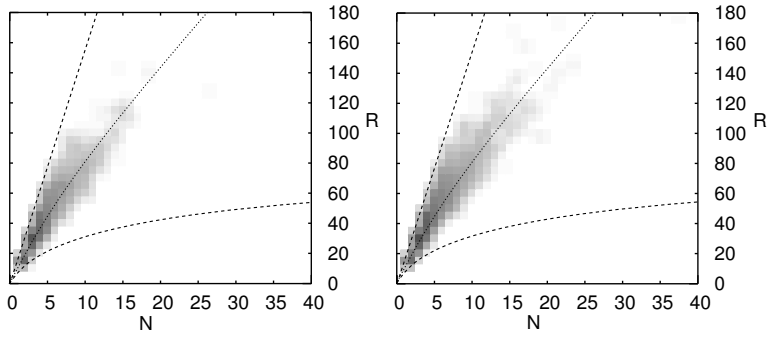

(a) $M = 1$, $Re = 0.0155$ (d) $M = 1$, $Re = 1.5529$

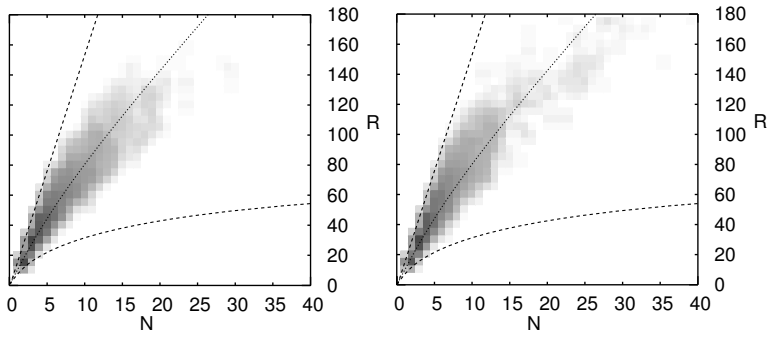

(b) $M = 10$, $Re = 0.0155$ (e) $M = 10$, $Re = 1.5529$

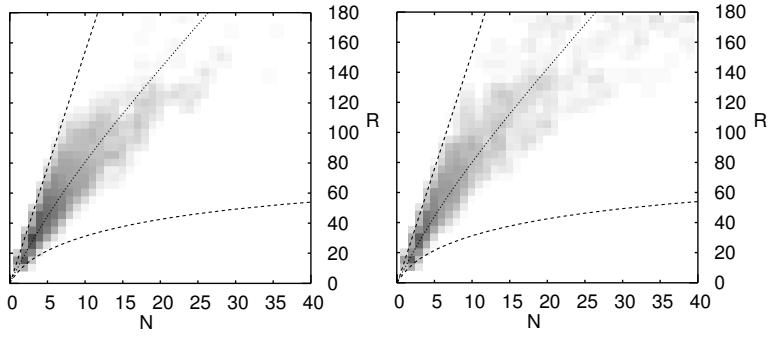

(c) $M = 100$, $Re = 0.0155$ (f) $M = 100$, $Re = 1.5529$

Figure 5.3: Probability density to find a cluster consisting of N particles and a radius of gyration of R for the same parameter sets as in Fig. 5.1 and Fig. 5.2. Regardless the mass density ratio M and Reynolds number, an average fractal dimension of $D = 1.15$ can be found which agrees for all M and Re within statistical errors. The low value of D illustrates the tendency of clusters to assume elongated shapes. The dashed lines show the extreme cases of a straight chain of particles and that of densest packing.

Cluster Size Distribution and Typical Cluster Size

In Fig. 5.4 the distributions $p_c(N)$ of the cluster size are shown for the considered combinations of mass density ratios M and Reynolds numbers Re which are defined as the probability to find a cluster of certain mass N. While for $M = 1$ the increase of the Reynolds number only slightly effects $p_c(N)$ for larger M an increase of the Reynolds number results in a $p_c(N)$ which is much more stretched towards larger cluster sizes N. This agrees with the overall appearance of particle distributions in Fig. 5.1 and the findings for the cluster pair distributions in Fig. 5.2. To characterize the distributions $p_c(N)$ we used the prediction for $p_c(N)$ from the kinetic clustering model (KCM) [209] which describes a power law decay for small N and an exponential tail, i.e.

$$p_c^{\mathrm{KCM}}(N) = C^{\mathrm{KCM}} N^{-3/2} \exp\left(-\frac{N}{N_t}\right), \tag{5.1}$$

and fitted it to the simulation results obtaining a parameter N_t for the stretch of the exponential part and a normalization factor C^{KCM}. Despite being based on the very simple assumption of randomly distributed particles and not taking any hydrodynamical interaction into account the distributions (5.1) resulting from the KCM model can be very well matched to our data for all combinations of M and Re. A similar functional form for the distribution of cluster sizes can even be found for spherical and RBC-like particles [212]. The KCM model also makes predictions for N_t as a function of the volume fraction ϕ which can be very well matched to findings from simulations for low Reynolds numbers [209]. However, it fails to predict N_t for higher Re as a consequence of neglecting hydrodynamical interactions. In any case, the functional form of $p_c^{\mathrm{KCM}}(N)$ allows the definition of N_t as the typical cluster size at which the crossover between the power law and exponential decay takes place.

In Fig. 5.5 the obtained N_t for all combinations of M and Re are plotted over the Stokes number $St = MRe$. Except for the data for $M = 1$ all typical cluster sizes N_t agree very well with a power law scaling

$$N_t - N_t^0 \sim St^{1/2} \tag{5.2}$$

with an offset of $N_t^0 \approx 1.7$. The rather small deviations for large N_t can be explained by the finite size of the considered system. Although N_t is always less than half the system size L the probability for the existence of clusters comparable to L is non-zero and is enhanced through the application of periodic boundaries. When fitting (5.1) to the data this might lead to an overestimation of the real N_t. Explaining the deviations from the scaling (5.2) for $M = 1$ is not so straightforward. It might be related to the leveling of particle and fluid inertia so that particle inertia plays a role subordinate to that of the fluid in particle clustering.

In the simulations also stresses of the fluid as well as solid phase were evaluated to obtain the apparent viscosity ν_{app} of the suspensions for the considered mass density ratios M and Reynolds numbers Re. For this the procedure described in Sec. 4.4.2 based on the method presented in [115] was applied. In Fig. 5.6 ν_{app} normalized by the viscosity increase due to the volume fraction of $\phi = 0.4$ is shown for all M and Re considered in this work. In all cases we find shear-thickening but much more pronounced the larger M. When plotted over the Stokes number

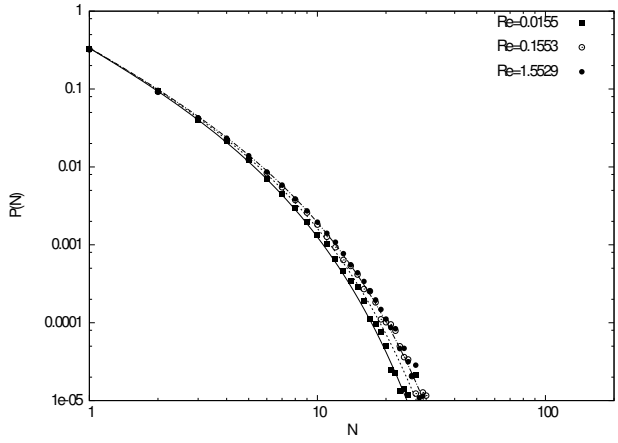

(a) $M = 1$

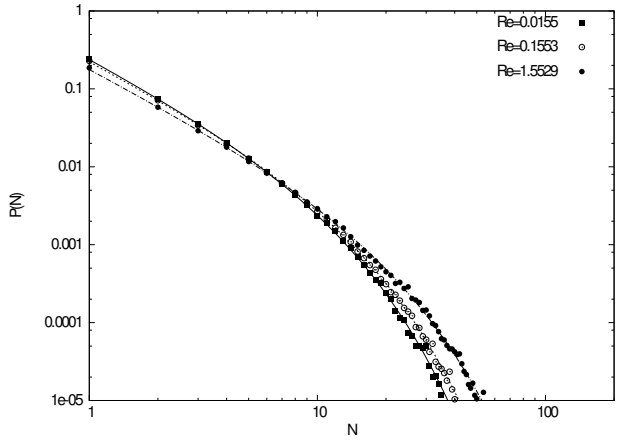

(b) $M = 10$

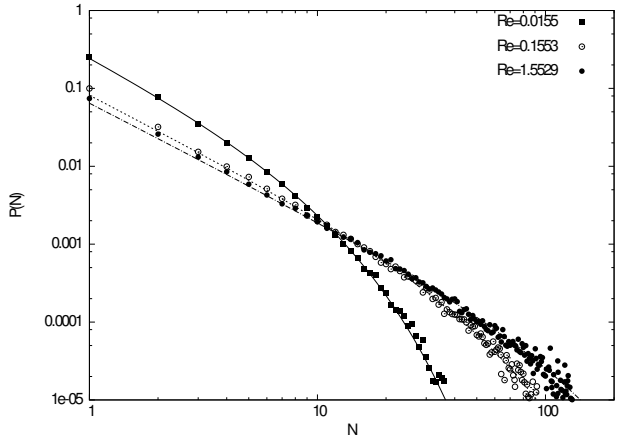

(c) $M = 100$

Figure 5.4: Cluster size distributions $p_c(N)$ for a set of mass density ratios M and Reynolds numbers Re as obtained by LBM simulations. The lines correspond to (5.1) fitted to the data.

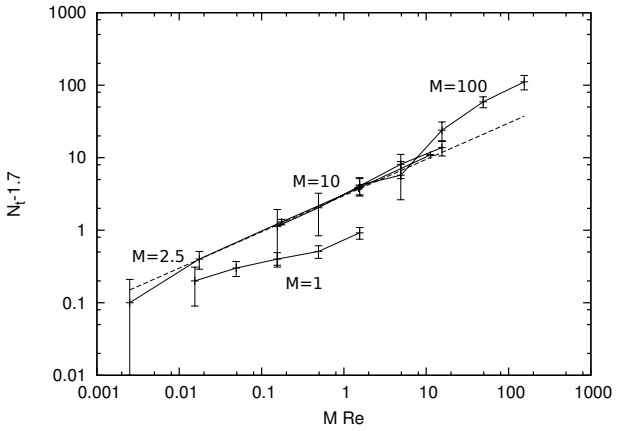

Figure 5.5: The typical cluster size N_t as a function of MRe for all considered combinations of mass density ratios M and Reynolds number Re. Except for the data for $M = 1$ which lies significantly below the other data for $M > 1$, and the highest typical cluster sizes, all data points collapse very well to a power law with exponent 1/2 (dashed line). The deviations from it for $M = 1$ could be explained by a too weak particle inertia in comparison to that of the suspending fluid. The upwards shift at large MRe for $M = 100$ might be a result of finite system size.

$St = MRe$ all curves fall on top of each other, i.e. for a given ϕ[4] a master curve for shear-thickening exists which scales with St. A small systematic deviation towards higher ν_{app} can be found for $M = 1$.

When ν_{app} is plotted as a function of the typical cluster size N_t (Fig. 5.7) we find that all data collapse within statistical errors to one curve which scales as $\nu_{\text{app}} \sim N_t^{0.4}$. Together with the other findings of this section this gives rise to the assumption that particle inertia plays the dominant role in shear-thickening. When particles approach each other in sheared flow they come the closer the higher their own inertia compares to that of the fluid. The decelerating effect of the fluid on the particle dynamics scales linearly with the fluid mass density. Once that particles have come very close lubrication forces lead to a strong bond between the particles which can only be loosened by accelerations due to interaction with other heavy particles. The mediating long range action of hydrodynamical forces becomes less important in this process. As a consequence clusters preferably aligned in compression direction of the shear flow are formed from solid particles which serve as a much more direct mechanism to transport momentum through the system.

In the following sections we first will take a step back and study the dynamics of two particles approaching each other in a shear flow in dependence on $\dot{\gamma}$ and M. We will then try to formulate a theory on how clusters of more than two particles form and break and will derive a distribution of cluster sizes, again as a function of $\dot{\gamma}$ and M. The aim of it is to understand the role of particle clustering in shear-thickening by relating resulting predictions for the typical cluster size $N_t(\dot{\gamma}, M)$ to the apparent viscosity as a function of these parameters.

[4]Of course, shear-thickening is very sensitive to ϕ, see Sec. 4.1.

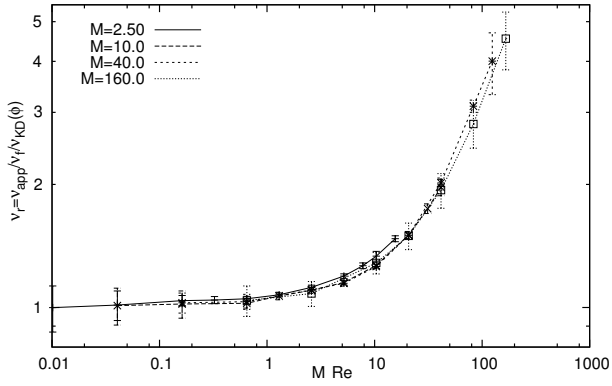

Figure 5.6: Shear-thickening curves for different mass density ratios M. When plotted over the Stokes number $St = MRe$ the curves collapse.

5.2 2-Particle Collision Model

5.2.1 Trajectories

To investigate how close two suspended particles get in a shear flow and to quantify the probability that they are found to fulfill the cluster criterion we set up a simple toy model of two particles approaching each other in a shear flow with shear rate $\dot{\gamma}$. Resembling a monodisperse two-particle suspension both particles have the same radius R_p and same mass m. Initial conditions are such that the velocities of each particle equals the local shear flow velocity, i. e. $\dot{\mathbf{r}} = (\dot{\gamma}y, 0)$. The initial positions are chosen such that $\mathbf{r}_1(t = 0) = (24d, d)$ and $\mathbf{r}_2(t = 0) = -(24d, d)$ creating a symmetric situation with the center of mass at $\mathbf{r} = (0, 0)$. In dependence on the parameter d the particles will approach each other and will scatter due to hydrodynamical interactions.

Hydrodynamical interactions between two particles can be approximated by a linear approximation of the lubrication forces that is valid for small particle distances. In 2D the resulting forces on each of two particles that move in respect to each other have the form:

$$\mathbf{F}_{\text{lub}} = m\ddot{\mathbf{r}}_i = -C\frac{\dot{h}}{h}\mathbf{e}_{ij} \qquad \text{with} \qquad h = |\mathbf{r}_j - \mathbf{r}_i| - 2R_p = r_{ij} - 2R_p. \tag{5.3}$$

Additionally, the particles feel a force due to the friction (Stokes, linear) with the homogeneous shear flow background, reading

$$\mathbf{F}_{\text{fric}} = m\ddot{\mathbf{r}}_i = D(\dot{r}_{i,y} - \dot{\gamma}r_{i,y})\mathbf{e}_x. \tag{5.4}$$

Mass of a particle and the drag force coefficient form an equivalent to the mass density ratio, i.e. $M \sim m/D$. With the dissipative action of lubrication alone, the particles would come to a halt if friction with a background at non-zero velocity would not drive them further with the shear flow. In Fig. 5.8 trajectories are shown for several combinations of the parameters $\dot{\gamma}$ and m. For small values of $\dot{\gamma}$ and m, particles continue their movement after the interaction with the other particle as if

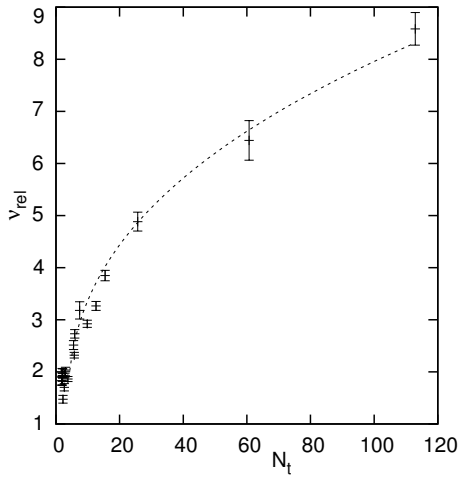

Figure 5.7: Correlation between relative apparent viscosity $\nu_{\mathrm{rel}} = \nu_{\mathrm{app}}/\nu_{\mathrm{f}}/\nu_{\mathrm{rel,KD}}$ and the typical cluster size N_t, where $\nu_{\mathrm{rel,KD}}$ is the relative apparent viscosity as a function of ϕ, (4.1).

no interaction had taken place. They arrive at the same $y = d$ at which they had been released and traveled the same distance in x-direction resembling the perfect symmetry known for the Stokes limit. If $\dot{\gamma}$ and/or m are increased, the symmetry of the trajectories is broken. The two particles come much closer to each other in approaching direction but are repelled so that their distance is larger when they depart. Also, their final separation in y-dimension can be found to be smaller than that at time $t = 0$. If $\dot{\gamma}$ and m is increased further, the particles lose so much relative speed due to the lubrication dissipation that the Stokes friction with the fluid background is not strong enough to separate them again. Instead they begin to tumble.

5.2.2 Two-Particle Sticking Probability

Cluster Condition, Sticking Time

Along some of the trajectories particles are that close that they fulfill the clustering condition $r_{12} < 2.2R_p$ which is derived from the maximum in the particle distribution function in a hard-sphere suspension. To define a probability that particles might be in such a state at every time step it is checked if this condition is fulfilled, and if so, a *sticking time* is increased by the time step of the integration Δt and normalized by the size of the time frame $T_{\dot{\gamma}}$. This procedure is equivalent to an integration definition

$$\tau = \frac{1}{T_{\dot{\gamma}}} \int_0^{T_{\dot{\gamma}}} \begin{cases} 1, & \text{if } r_{12} < 2.2R \\ 0, & \text{else} \end{cases} \mathrm{d}t. \tag{5.5}$$

We can interpret τ as the probability that the two particles will stick for a collision parameter d in dependence of the parameters $\dot{\gamma}$ and m.

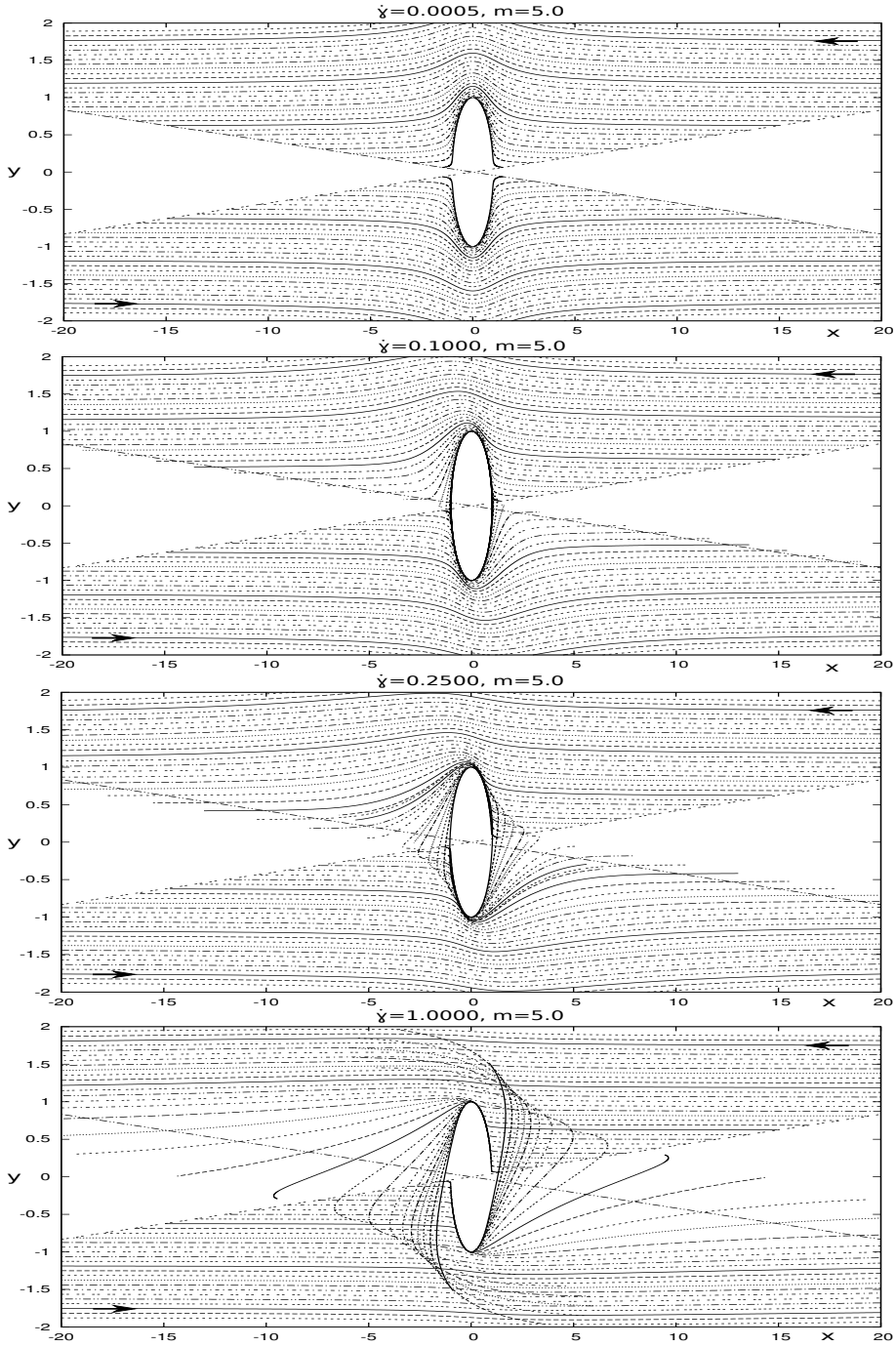

Figure 5.8: Trajectories of two particles approaching each other in a shear flow with a collision parameter d for a few chosen parameter sets $(\dot{\gamma}, m)$.

Number Density of Collision Partners as Function of d

We are looking for a distribution $P(d)$ that tells us how many particles would actually follow the trajectories of Sec. 5.2.1, and could be actual collision partner, i.e. no other particle is closer at that time.

As d gets larger the difference in shear velocity between the two particles increases. In an area element $\Delta d \cdot l$, where $l = 48d$ is the stretch in x-direction that passes by in the time frame $T_{\dot\gamma}$, we will find

$$N_l = n(\phi, R) \cdot \Delta d \cdot 48d \tag{5.6}$$

particles.

A particle collides with another if their distance is not larger than $2R$. This results in a density of particles on one trajectory that is given by

$$n_{l,\mathrm{coll}} = 2R \cdot n(\phi, R). \tag{5.7}$$

We also could call this quantity line collision density.

The volume of a trajectory is given by its discretization in height, $\Delta d = 0.125$, and the length of an undisturbed trajectory, $48d$, i. e.

$$V_{\mathrm{coll}} = 48d \cdot \Delta d. \tag{5.8}$$

With this contribution we take into account the probability that a particle, able to collide with the other, will actually be found on such a trajectory. For small d, the velocity is small, too, and hence the number of particles that touch any point of the trajectory within $T_{\dot\gamma}$ is small.

The probability that d is the free path in the dimension $s = |(48d, d)| = \sqrt{d^2 + (48d)^2} \approx 48d$, meaning that this is the trajectory of an actual collision partner, is an exponential distribution

$$P(d) = 48 \ln \bar{s}_{1\mathrm{D}} \exp\left(-\frac{48d - 2R}{\ln \bar{s}_{1\mathrm{D}}}\right), \qquad d \le 2R, \tag{5.9}$$

with a typical mean $\bar{s}_{1\mathrm{D}}(\phi) = 1/n$ resulting from the particle density n which, in turn, is derivable from the volume ration and radius, $n(\phi, R) \sim \phi/R^2$.

Multiplying all the densities/probabilities we arrive at the final expression for the average number of particles that might be collision partners during the time frame $T_{\dot\gamma}$ in dependence on d,

$$N(d) = n(\phi, R)\Delta d \cdot 48d \cdot 48 \ln \bar{s}_{1\mathrm{D}} \exp\left(-\frac{48d - 2R}{\ln \bar{s}_{1\mathrm{D}}}\right). \tag{5.10}$$

This quantity contains all geometrical information based on ϕ and R.

In Fig. 5.9 curves for $\tau(d)$ that are measured for the same parameter sets $(\dot\gamma, m, \phi = 0.4)$ as in Fig. 5.8 are shown together with three realizations of (5.10).

Sticking Probability

To arrive at an overall probability of sticking in dependence of only the parameters $\dot\gamma$, m and ϕ we have to integrate the product of $\tau(d)$ and $N(d)$, i.e.

$$P_0 = \int_0^\infty \tau(d) \cdot N(d)\ \mathrm{d}d \tag{5.11}$$

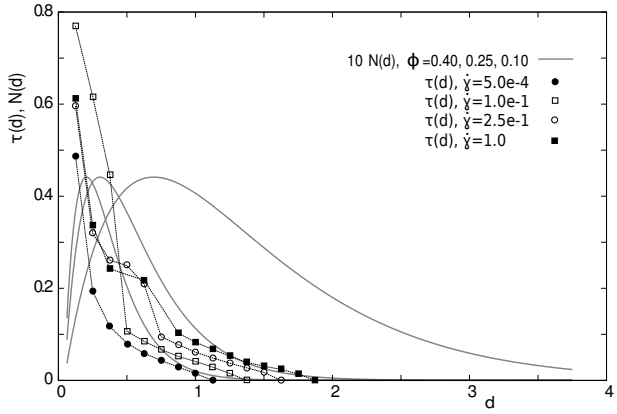

Figure 5.9: Sticking time $\tau(d)$ for a range of $\dot{\gamma}$ and fixed $m = 5.0$. Also shown is the number density of collision partners $N(d)$ for $\phi = 0.1, 0.25, 0.4$.

over all collision parameter d. However, the probability that two particles fulfill the cluster condition is guaranteed to be zero for all $d > 2R$, so a numerical integration can be truncated at a finite $d > 2R$ with no additional error.

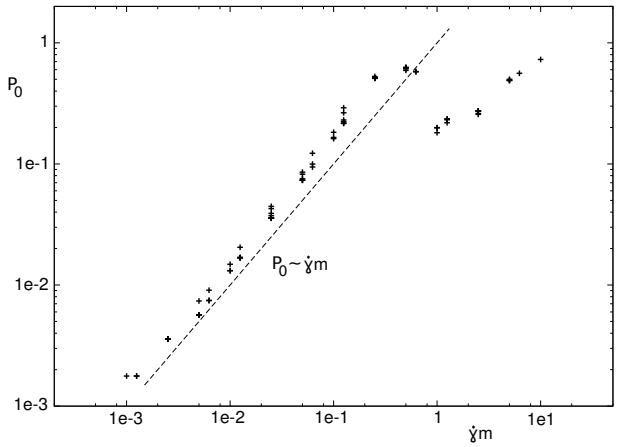

Figure 5.10: P_0 as a function of $\dot{\gamma}m$. P_0 increases as $\sim (\dot{\gamma}m)^b$ with $b \approx 1$. The origin of the decrease and the subsequent repeated increase is (probably) a consequence of the finite integration time of the two-particle system where for higher shear rates particles "touch" each other for a second time.

In Fig. 5.10 $P_0(\dot{\gamma}, m, \phi = 0.4)$ is shown over a wide range of $(\dot{\gamma}, m)$. P_0 increases as $\sim (\dot{\gamma}m)^b$ with $b \approx 1.25$ for a wide range but is followed by a decrease and a subsequent increase. The later behavior might be related to the humps in $\tau(d)$ (see Fig. 5.9) that could be, in turn, an artifact of the finite $T_{\dot{\gamma}}$.

5.3 Statistical Clustering Model

In a sheared suspension particles might fulfill the cluster condition, forming a 2-particle-cluster. Before such a cluster of size $N_1 = 2$ breaks due to the shear stress it might collide with another cluster of size N_2. Defining probabilities of sticking/merging and breaking of clusters depending on the cluster sizes $N_{1,2}$ and the parameters of the sheared system, $\dot{\gamma}$, m, ϕ, in this section we will set up a master equation for the probability $p_c(N)$ that a particle belongs to a cluster of size N based on these probabilities.

5.3.1 Elementary Processes

The change of the probability to find a cluster of size N can be caused by a number of elementary processes.

Merging of smaller clusters

A cluster of size N can be formed from 2 clusters of sizes N_1 and $N - N_1$. The probability that such clusters of size N_1 and $N - N_1$ exist is $p_c(N_1)$ and $p_c(N - N_1)$, respectively. The probability that they actually collide and stick is given by $P_{\text{stick}}(N, N_1)$ which depends on the set of system parameters. A cluster of size N can be formed by any possible combinations of N_1 and $N - N_1$, that is, the probability that a cluster of size N forms through merging of two other clusters of any possible sizes can be given by

$$P_{\text{merge}} = \sum_{N_1=1}^{N-1} p_c(N_1) p_c(N - N_1) P_{\text{stick}}(N, N_1). \tag{5.12}$$

Breaking of larger clusters

The probability that a cluster of size $N_0 > N$ breaks into two parts one of which is of size N, thus the result of splitting, is modeled as

$$P_{\text{split}} = \sum_{N_0=N+1}^{\infty} \dot{\gamma} N_0^{1/D-1} p_c(N_0). \tag{5.13}$$

Several assumptions have been made here. First, we assume that the probability that a cluster breaks is proportional to the shear rate $\dot{\gamma}$, which is reasonable because $\dot{\gamma}$ defines a time scale. Second, we assume that the larger a cluster is the more sensible it is to strain. We could combine these two assumptions in another formulation of the argument: the product $\dot{\gamma} R_c$ is proportional to the strain on the cluster and breaking is linear dependent on that. As found in a previous investigation of cluster sizes, clusters in shear flow mostly are elongated in one direction (typically diagonal) leading to a dimensional relation $N = R_c^D$ with a fractal dimension of $D \approx 1.15$. The additional -1 in the exponent stems from the combinatoric fact that N combinations of N_1 and $N_2 = N - N_1$ exist into which a cluster of size N can break (including the case where $N_1 = 0$ or $N_2 = 0$). Hence the probability that the mother cluster breaks into a certain combination (N_1, N_2) has to be divided by N. Every resulting combination is assumed to have the same probability.

Absorption into larger cluster

One of the processes that decrease the number of clusters of size N is the formation of a larger cluster of size $N_0 > N$ by merging the cluster of size N with another cluster of size $N_0 - N$. The probability of such a process is

$$P_{\text{absorb}} = \sum_{N_0=N+1}^{\infty} p_c(N) p_c(N_0 - N) P_{\text{stick}}(N_0, N). \tag{5.14}$$

Dissolving into smaller clusters

The second process that decreases $p_c(N)$ is the breaking of the cluster of size N into two smaller clusters of sizes N_1 and $N_2 = N - N_1$. With the assumption that all results, (N_1, N_2), are equally probable, the probability of such a dissolving process is readily summed up (over all $N_1 < N$) to

$$P_{\text{dissolve}} = \sum_{N_1=1}^{N-1} p_c(N) \dot{\gamma} N^{1/D-1} = p_c(N)(N-1)\dot{\gamma} N^{1/D-1}. \tag{5.15}$$

Here again, we made the same assumptions on breaking behavior as for P_{split}.

5.3.2 Master Equation for $p_c(N)$

We now can add up positive and negative processes for $p_c(N)$ in a master equation for its dynamics.

$$\partial_t p_c(N) = P_{\text{merge}} + P_{\text{split}} - P_{\text{absorb}} - P_{\text{dissolve}} \tag{5.16}$$

The dynamics can be solved numerically, starting from an initial condition that fulfills the condition $\sum_{N=1}^{\infty} p_c(N) = 1$. We have chosen $p_c(1) = 1$ and $p_c(N > 1) = 0$ resembling a system with randomly distributed particles none of which is in contact with another. Solving the master equation iteratively the distribution of cluster sizes $p_c(N)$ will converge to an equilibrium solution.

Crucial for the dynamics and equilibrium form of $p_c(N)$ is the sticking probability of two clusters, i.e. $P_{\text{stick}}(N = N_1 + N_2, N_1)$. We assume that P_{stick} takes a functional form

$$P_{\text{stick}} = \beta^b N^{1/D} \qquad \text{with} \quad \beta = C\dot{\gamma} m \tag{5.17}$$

according to the findings in Sec. 5.2.2. Despite some remaining unclarity for large $\dot{\gamma} m$ the exponent $b = 1.25$ has been used here. The assumption $P_{\text{stick}} \sim N^{1/D}$ stems from a spatial scaling argument, treating clusters of radius $R = N^{1/D}$ as particles with the same radius. Here, the result $D = 1.15$ from Sec. 5.1.2 was used.

Results and Discussion

Obtaining an analytical solution for $p_c(N)$ from (5.16) proves difficult. We therefore have numerically integrated the master equation (5.16) in an iterative fashion (Euler method) and found stable equilibrium solutions for $p_c(N)$ after approximately 10^4 time steps. The distribution has initially been set to $p_c(1) = 1$ and $p_c(N) = 0$ for all $N > 1$. The summations in (5.13) and (5.14) have been truncated at $N = 500$ which has been found not to introduce significant errors when

compared to a reference integration with a upper limit of $N = 10^5$. A least-squares fit routine was coupled to the solver for (5.16) in which β was varied so that the resulting $p_c(N)$ matches the cluster size distributions as obtained from the LBM simulations for different mass density ratios M and Reynolds numbers Re as described in Sec. 5.1.2. For the simulation data the KCM prediction (5.1) was used to determine a typical cluster size N_t.

The statistical clustering model presented in this section results in $p_c(N)$ that show a very good agreement with the KCM model, which was used as a reference here, as shown in Fig. 5.11. By varying $\beta = C\dot{\gamma}m$ in the sticking probability function (5.17) the outcome of the numerical integration can be matched to the results $p_c^{\mathrm{LBM}}(N)$ from the LBM simulations as reported in Sec. 5.1.2.

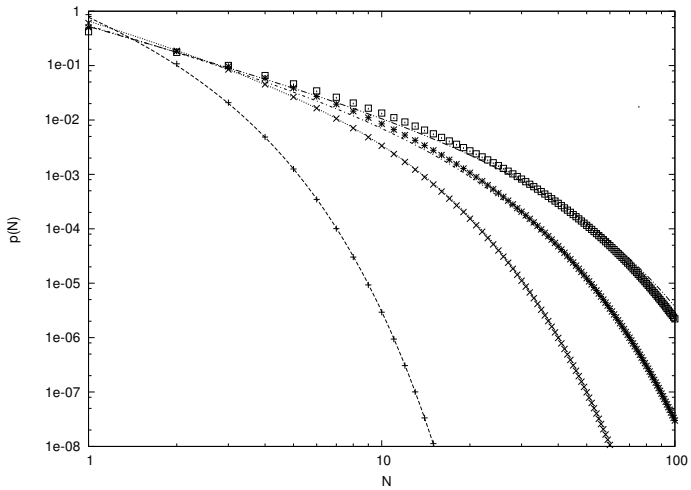

Figure 5.11: Equilibrium cluster size distribution $p_c(N)$ for different β in (5.17) (data points) matching results of the KCM model (lines) for a number of typical cluster sizes N_t. For larger N_t an increasing deviation can be observed.

However, when the typical cluster size N_t obtained from fits of $p_c^{\mathrm{KCM}}(N)$ to $p_c^{\mathrm{LBM}}(N)$ are plotted against the parameters β obtained from fits of the statistical clustering model we see a strong deviation from the behavior $N_t \sim \beta^{1/2}$ as could be expected from the scaling $N_t \sim MRe^{1/2}$ found for the LBM results shown in Fig. 5.5. In Fig. 5.12 the relation $N_t(\beta)$ is plotted together with the expected power law. For small β the typical cluster size $N_t(\beta)$ does indeed behave as a power law with an exponent $\approx 1/2$. For larger β an increasing deviation from this behavior can be observed. For the largest β studied here it even increases much faster than exponentially. The clustering model was based on clustering behavior found in a 2-particle problem. It might therefore well be that the made assumptions are reasonable as long as the typical cluster size is small. For larger clusters, and therefore direct interaction of more than two particles, corrections to this behavior will be necessary.

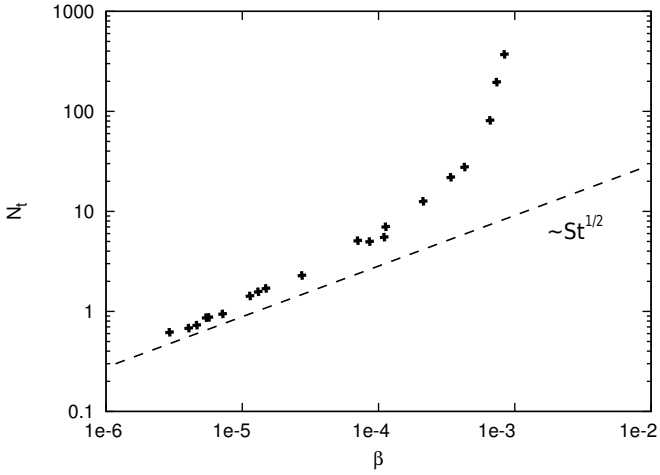

Figure 5.12: Typical cluster sizes N_t as a function of $\beta = C\dot{\gamma}m$ in (5.17) as obtained from fits of the cluster size distribution from the KCM model (5.1) to the numerical solutions of (5.16). For small β, $N_t(\beta)$ agrees with the scaling $N_t \sim St^{1/2}$ found in full simulations and shown in Fig. 5.5. An increasing deviation, with eventual divergence, from this behavior can be found for all other values of β.

5.4 Discussion

In this section we have reported measurements of the microstructure of sheared monodisperse hard-sphere suspensions in shear flow realized by means of the Lattice-Boltzmann method. We concentrated on dense suspensions with a volume fraction $\phi = 0.4$ for which a clearly visible continuous shear-thickening behavior can be expected. Unlike other works on shear-thickening suspensions, in this chapter we focused on the changes resulting from variations of the particle shear Reynolds number $Re = 0.00155..1.5529$ for different mass density ratios $M = \rho_s/\rho_f = 1..100$. In measurements of a cluster pair distributions for the range of considered Re and M we saw that the expected breaking of the symmetry in the pair distribution function occurs clearly at $Re > 1$ only for density ratios $M > 1$. With the increase of M also the increase of the overall amplitude of the cluster pair distribution function with Re was found much more pronounced. In measurements of cluster distributions this tendency could be recovered and quantified by the finding that the typical cluster size scales with the Stokes number $St = MRe$ as $N_t \sim St^{1/2}$. This Stokes number scaling we also could report for shear-thickening measurements for a set of M. These finding give rise to the assumption that particle inertia plays a dominant role in shear-thickening suspensions, a fact has not been discussed extensively in the literature.

From measurements of the distributions of the radius of gyration linked to the number of particles in clusters forming in sheared suspensions we find a fractal dimension of $D = 1.15$ for all considered combinations of M and Re suggesting that the geometrical properties of the clusters do not change when these system parameters are varied. Together with the asymmetry found in the pair distribution

function this fact characterizes particle clusters as preferably of chain-like shape (instead of compact globule-like clustering) and as oriented preferably in the direction of compression in the shear flow. This supports the assumption that particle clusters offer an effective mechanism through which momentum can be transfered through the system. When the apparent viscosity ν_{app} of the suspension is plotted as a function of the typical cluster size N_t we indeed find that all data points collapse to one curve regardless the parameters Re and M which scales as $\nu_{\text{app}} \sim N_t^{0.4}$.

Aiming at investigating the process of cluster formation in this chapter we modeled the approach of two particles in a shear flow from which an integrated time was derived in which the particles fulfill the cluster criterion. The probability to find a two particles clustering in dense suspensions that could be derived from that was also found to obey Stokes number scaling but with slightly larger exponent $b = 1.25$. When this behavior of the probability for clustering particles is then used in a statistical clustering model which models probabilities of mechanisms of cluster formation and dissolution as functions of the shear rate and under usage of the spatial scaling assumption that particle cluster with a radius of gyration $R \sim N^{1/D}$ behave as single particles when they collide, a cluster size distribution function can be obtained in dependence on the shear rate and mass density ratio. The results agree very well with the predictions of the KCM model which serves as a reference and a way to extract a typical cluster size N_t from the distributions. The KCM model, however, is only valid for $Re \ll 1$. The statistical clustering model is successful in reproducing the form of $p_c(N)$ also found in the LBM simulations by varying the shear rate $\dot{\gamma}$ and mass density ratio M. For small β it does reproduce the scaling $N_t \sim St^{1/2}$ observed through fully-resolved LBM simulations. For larger β increasing deviations are present, a clear hint that higher order particle-particle interactions have to be taken into account. The scaling assumptions deduced from the two-particle model, and the assumption that cluster-cluster collisions can be modeled as particle-particle collisions might be valid for small N_t but corrections are clearly necessary for larger N_t.